Journal of Fluids and Structures (1999) **13,** 1097–1112
Article No.: jfls. 1999.0246, available online at http://www.idealibrary.com on IDEAL®

CFD ANALYSIS OF TURBULENT FLOW PAST SQUARE CYLINDER USING DYNAMIC LES

S. MURAKAMI AND S. IIZUKA

Institute of Industrial Science, University of Tokyo, 7-22-1 Roppongi, Minato-ku, Tokyo, 106, Japan

AND

R. OOKA

Faculty of Engineering, Fukui University, 3-9-1 Fukui-shi, Fukui, 910, Japan

(Received 12 November 1998 and in revised form 15 July 1999)

Computational fluid dynamics (CFD) analysis of turbulent flow past a square cylinder is conducted using large eddy simulation (LES). In the first part of the paper, the implementation of the three-dimensional (3-D) LES computation based on the conventional standard Smagorinsky model (S model) shows a good prediction capability compared with that of turbulence models based on Reynolds-averaged Navier-Stokes equations (RANS models). Next, the computation using the dynamic Smagorinsky model (DS model) is carried out, and the improvement by the use of DS model is described. Lastly, the Lagrangian dynamic Smagorinsky model (LDS model) is introduced to overcome the disadvantages of DS model, e.g., calculation instability. Results obtained from the various SGS models are compared with those from experiments.

1. INTRODUCTION

RECENTLY, THE RELATIVE PERFORMANCE of various turbulence models, i.e. the standard k-ε model, algebraic stress model (ASM), Reynolds stress model (RSM) and LES have been examined in bluff body aerodynamics applications (Murakami *et al*. 1992, 1993; Murakami 1993). The flowfield around a bluff body is highly complex, since it consists of separation at the front corners, recirculation, vortex shedding, etc. We have clarified that LES is the most suitable tool for analysing the complicated flow situations usually treated in applications of bluff body aerodynamics. This paper reports on the recent developments in LES techniques applicable to CFD in the research field of bluff body aerodynamics, and presents results of analysis based on LES applied to unsteady flow phenomena past a square cylinder.

2. FLOWFIELD ANALYSED: 3-D CHARACTERISTICS OF FLOW PAST SQUARE CYLINDER

This paper is concerned with turbulent vortex shedding past a long square cylinder, which is 2-D in the mean. When the flowfield is 2-D in the mean, the unsteady flowfield is frequently solved by unsteady 2-D computations in the field of engineering applications because CPU time is reduced greatly as compared to 3-D computations. Figure 1 compares the power spectrum given by 2-D and 3-D LES computations with experimental results (Vickery 1966). The spectrum shapes of lift force, F_L, and drag force, F_D, given by the 3-D computation correspond very well to those from the experiment. On the other hand, the

0889–9746/99/101097 + 16 $30.00

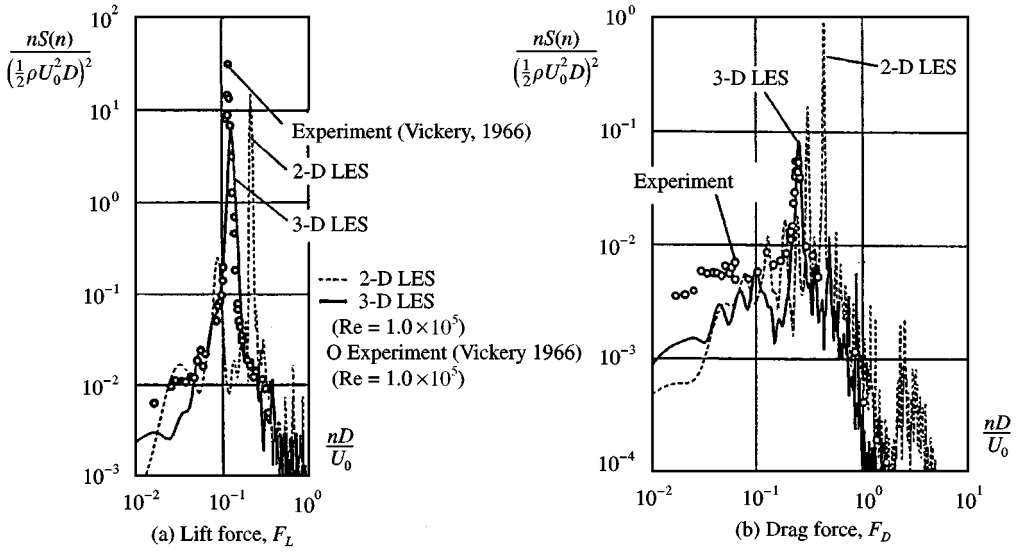

Figure 1. Power spectra of fluctuating lift and drag force.

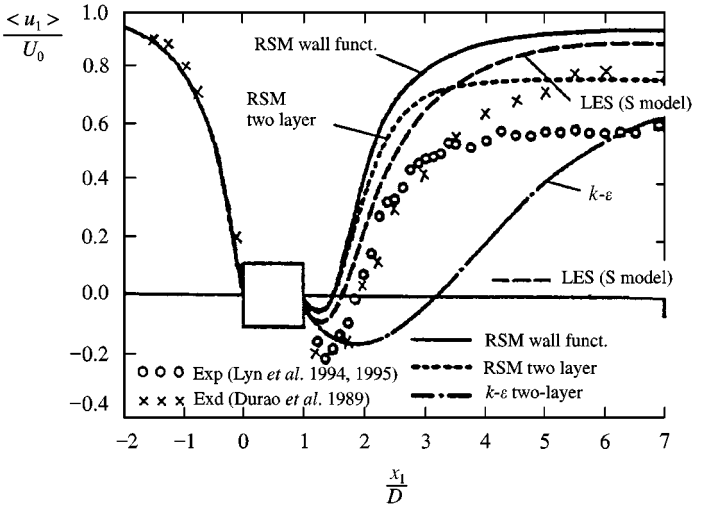

Figure 2. Comparison of time-averaged velocity $\langle u_1 \rangle$ along the centreline.

peak frequencies of lift force and drag force in the 2-D computation deviate greatly from the experimental results. These large discrepancies in the results of 2-D LES are not surprising because the instantaneous structure of the flowfield is highly 3-D. Thus, its effects cannot be reproduced at all by 2-D LES computations. Hereafter, analysis by 3-D LES computations will be presented.

Results for the flowfield around a 2-D square cylinder at $\mathrm{Re} = 2{\cdot}2 \times 10^4$ predicted by the major turbulence models, i.e., the standard k-ε model (Launder & Spalding 1974), RSM (Launder *et al.* 1975; Craft & Launder 1992), and LES [based on the conventional standard Smagorinsky model (S model) (Deadorff 1970, 1972)] are compared in Figure 2. For this

flowfield, the detailed experiment was carried out by Lyn and Rodi (1994) and Lyn *et al.* (1995) and this flow was used as the test case for recent LES workshops (Rodi *et al.* 1996; Voke 1997). In our experience, 3-D LES shows the best agreement with experimental data, even though the conventional S model is used. Next is RSM, while the standard k-ε model gives the poorest results. Figure 2 shows the general tendency of the relative performance of these models; this is similar for other flowfields, i.e., for flow around other types of bluff bodies, such as a cube (Murakami 1993).

3. A NEW TOPIC FOR LES: DEVELOPMENT OF DYNAMIC LES

3.1. Shortcomings of the Standard Smagorinsky Model and Advantages of the Dynamica Model

The S model (standard Smagorinsky model) has been widely used in the computation of LES since the pioneering work of Deardorff (1970). In the S model, a simple eddy-viscosity type assumption is used for modeling the sub-grid scale (SGS) stress τ_{ij}, as detailed in the following.

(i) SGS stress

$$\tau_{ij} = \overline{u_i u_j} - \bar{u}_i \bar{u}_j; \tag{1}$$

(ii) eddy-viscosity model in S model

$$\tau_{ij} - \tfrac{1}{3}\delta_{ij}\tau_{kk} = -2\nu_{SGS}\bar{S}_{ij}, \tag{2}$$

$$\nu_{SGS} = (C_S\bar{\Delta})^2|\bar{S}| \quad (C_S\text{: } 0{\cdot}1\text{–}0{\cdot}25), \tag{3}$$

$$\bar{S}_{ij} = \frac{1}{2}\left(\frac{\partial \bar{u}_i}{\partial x_j} + \frac{\partial \bar{u}_j}{\partial x_i}\right), \quad |\bar{S}| = (2\bar{S}_{ij}\bar{S}_{ij})^{1/2}. \tag{4}$$

The S model is so simple and well-designed that it has been applied to many flowfields and has attained great success. However, the S model has several shortcomings; e.g., (a) the S model is overly dissipative, (b) the Smagorinsky constant, C_S, must be optimized for each flowfield, etc.

The Smagorinsky constant, C_S, in the S model is optimized from 0·1 to 0·25 for various flowfields (Schumann 1975; Clark *et al.* 1979; Monsour *et al.* 1979; Antonopoulos-Domis 1981; Biringen & Moin 1981; Moin & Kim 1982; Horiuti 1987; Mason 1989; Mason & Derbyshire 1990; Mizutani *et al.* 1991). As was already pointed out, the flowfield around a bluff body includes various types of flow properties such as impinging, separation, free shear layer, vortex shedding, etc. Thus, it is not easy to select one adequate value of C_S for analysing the flowfield around a bluff body. Therefore, the shortcoming of using a constant value of C_S becomes serious in CFD applications for bluff body aerodynamics.

To correct the drawback of a constant value of C_S, several models have been proposed. The most successful is the well-known dynamic model which was proposed by Germano *et al.* (1991) and revised by Lilly (1992). In the standard dynamic Smagorinsky model (hereafter called DS model for short), $C(=C_S^2)$ is determined as a variable of space and time following the properties of the flowfield, using two filters with different characteristic scales: a grid filter and a test filter (Germano *et al.* 1991), cf. equations (A1) and (A2) in Appendix A. This treatment of C is the first advantage of the DS model over the S model.

The second advantage of the DS model over the S model is the treatment near the wall. In the S model, the empirical model function f_μ (Van Driest 1956) is required for damping the

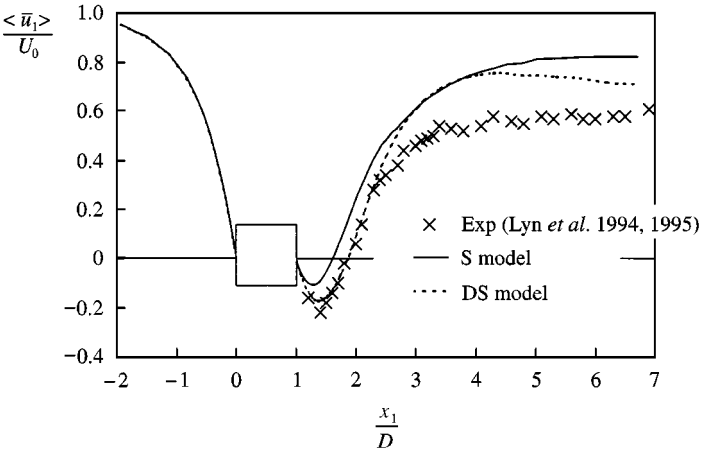

Figure 3. Comparison of time-averaged velocity $\langle \bar{u}_1 \rangle$ along the centreline between S model and DS model.

SGS viscosity, ν_{SGS} in the area near the wall,

$$\nu_{SGS} = (C_S \bar{\Delta} f_\mu)^2 |\bar{S}|, \quad f_\mu = 1 - \exp(-x_n^+/25). \tag{5}$$

In the DS model, f_μ is not necessary since the value of C automatically goes to zero in the laminar region just near the wall, and the model consequently becomes more elegant.

3.2. Comparison Between the S Model and the DS Model

The prediction accuracy of DS model is much improved compared to the result of conventional static S model, as is shown in Figure 3 (Murakami *et al.* 1997). In front of the cylinder, the results are not influenced by the difference of the SGS models used but large differences are observed in the wake region. The S model considerably underestimates the length of the reverse flow region. The DS model shows a better agreement with the experiment than the S model.

3.3. Difficulty with the DS Model

The DS model has significant advantages over the S model as described in the foregoing. However, the DS model still has several aspects that require improvement. One of these shortcomings is large fluctuations in C in the DS model. Since the fluctuations of $C(=C_S^2)$ are very large in the DS model, it is not easy to carry out stable computations. This drawback is particularly serious in the 3-D computation of bluff body aerodynamics.

3.4. Technique for Stabilizing Computations by the DS Model

In order to stabilize the fluctuations in C, various techniques and models have been proposed. Some of them are described below.

(i) Space or time averaging and clipping. When the flowfield has a homogeneous direction (e.g. channel flow), C is often calculated using the quantities averaged in the homogeneous direction. The technique of time averaging is also used sometimes (Akselvoll & Moin 1993). More simply, the technique of clipping is used, i.e. when C becomes negative, it is forced to zero.

(ii) Lagrangian dynamic model (Meneveau *et al.* 1994, 1996). The Lagrangian dynamic Smagorinsky model (hereafter referred to as the LDS model) proposed by Meneveau *et al.* (1994, 1996) introduced averaging along the flow path line rather than averaging over homogeneous directions. The length of averaging is a very important factor in the modelling. The details of LDS model are described in Appendix A.

4. PERFORMANCE OF LAGRANGIAN DYNAMIC SMAGORINSKY MODEL

4.1. Computed Cases

The computed cases here are summarized in Table 1. In this paper, two cases of LDS model computation are conducted. The LDS model is based on Lagrangian averaging of which the time scale is defined as $T = \alpha\bar{\Delta}I_{\mathrm{LM}}^{-1/4}(T = \alpha N, N = \bar{\Delta}I_{LM}^{-1/4})$ as shown in Appendix A. One is the case which adopts the time scale $T = 2N(\alpha = 2)$ as recommended by Meneveau *et al.* (1994) for isotropic turbulence (refer to Appendix A). The other is a case in which the time scale is reduced to 1/10 of the recommended value, i.e. $T = 0{\cdot}2N$ ($\alpha = 0{\cdot}2$) to investigate the effect of the value of T. A large value of T leads to a large contribution of the earlier upstream information since the time scale, T, determines the length of integration along a flow path-line. It can be anticipated that the appropriate time scale in complex flowfields, such as the flow around a square cylinder, is smaller than that in isotropic turbulence estimated by Meneveau *et al.* (1994) because the flow characteristics change rapidly in the flow near the cylinder. Hence, the computation with 1/10 value of the recommended time scale, T, for isotropic turbulence is tested.

4.2. Results

4.2.1. *Calculation Stability*

The required CPU time for various SGS models used here is also shown in Table 1. The required CPU time in application of the DS model is much larger than that used by the S model, since the S model is very stable. As described above, the large fluctuation of C in the DS model leads to calculation instability. Then, the computation of the DS model requires more CPU time. CPU time can be reduced remarkably by switching the SGS model from the DS to the LDS model. The reason is considered to be as follows. The Lagrangian averaging contributes to the stabilization of the fluctuation of C. Therefore, the computation of the LDS model becomes more stable than with the DS model, and CPU time in the LDS model is reduced remarkably. As shown in Table 1, the S model is very stable and the LDS model is quite stable. In contrast, the DS model is unstable.

Table 1

Computed cases and required CPU time

Type of SGS model	Averaging of C	Clipping	Required CPU time *
S	—	—	—
DS	Without	with	$\sim 4{\cdot}3$
LDS ($T = 2N$)	Lagrangian	without	$\sim 2{\cdot}2$
LDS ($T = 0{\cdot}2N$)	Lagrangian	without	$\sim 2{\cdot}2$

*Normalized by the CPU time required by S model.

4.2.2. *Time-averaged velocity*

Figure 4 shows a comparison of mean velocity vectors around a square cylinder. The sizes of reverse flow region near the side face of the cylinder are almost the same in both cases of the LDS model ($T = 2N$, $T = 0{\cdot}2N$) computations, and smaller than that of the DS model.

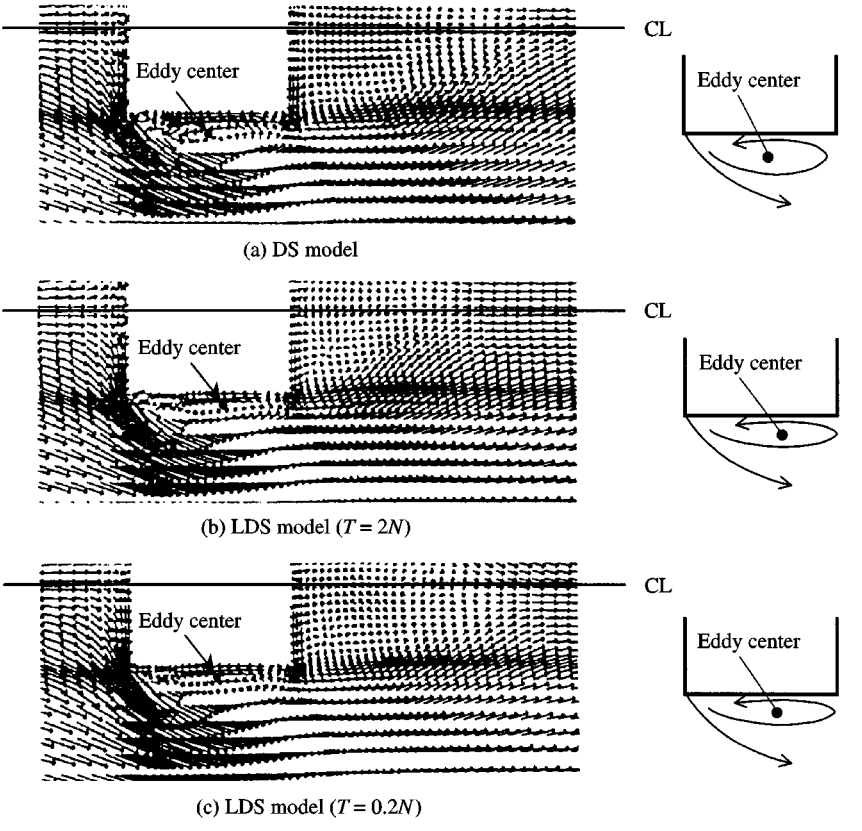

Figure 4. Time-averaged velocity vectors around a square cylinder.

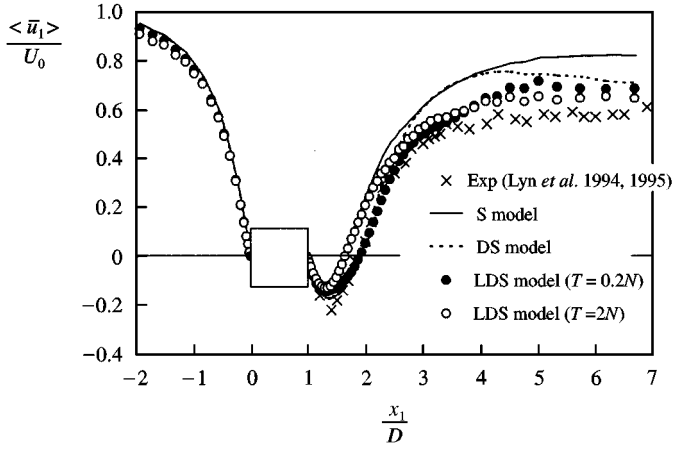

Figure 5. Comparison of time-averaged velocity $\langle \bar{u}_1 \rangle$ along the centre line for S, DS and LDS models.

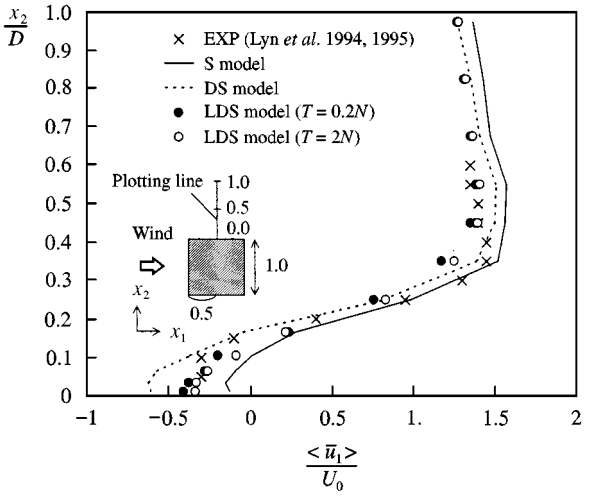

Figure 6. Comparison of time-averaged velocity $\langle \bar{u}_1 \rangle$ near the side-face for S, DS and LDS models.

The position of eddy centre in this reverse flow region is located leeward and near the cylinder to some extent in both the LDS model cases compared with that of the DS model.

Figure 5 illustrates the streamwise distribution of the time-averaged velocity, $\langle \bar{u}_1 \rangle$, along the centreline. The LDS model with $T = 2N$ considerably underestimates the length of the reverse flow region behind the cylinder in comparison with both the DS model and the experiment. On the other hand, the result of the LDS model with $T = 0{\cdot}2N$ remarkably improves accuracy and shows good agreement with the experiment in the region of $1 < x_1/D < 2$. Further downstream ($x_1/D > 3$), although the LDS model with $T = 0{\cdot}2N$ seems to give a more reasonable result than other SGS models compared here, the recoveries of streamwise velocity in all cases are more rapid than that in the experiment.

Figure 6 compares the lateral distributions of $\langle \bar{u}_1 \rangle$ along the line at the midpoint of the side face of the cylinder. In general, the results of both LDS model ($T = 2N$, $T = 0{\cdot}2N$) computations show good agreement with the experiment.

4.2.3. *Model coefficient* $\langle C \rangle^{1/2}$

Figure 7 illustrates the distributions of the model coefficient, $\langle C \rangle^{1/2}$, along the same line as Figure 6. In the S model, it corresponds to the value of $C_S (= 0{\cdot}13)$ multiplied by the Van Driest type dumping function f_μ. The $\langle C \rangle^{1/2}$ values predicted by both LDS model computations are generally smaller than that in the DS model. The values for the LDS models become larger than that for the S model near the cylinder, but the values of the LDS models are smaller than that of the S model in the region of $x_2/D > 0{\cdot}25$. Rapid decrease of $\langle C \rangle^{1/2}$ in the LDS model cases in the region far from the cylinder is mainly due to the fact that results of the LDS models are much more influenced by the upstream uniform flow in this region compared to the DS and S models.

4.2.4. *Reynolds shear stress*

Figure 8 shows a comparison of total shear stress, $\langle u_1' u_2' \rangle$, (GS + SGS) along the same line as in Figure 6. The results in both LDS model cases are quite different from those in the

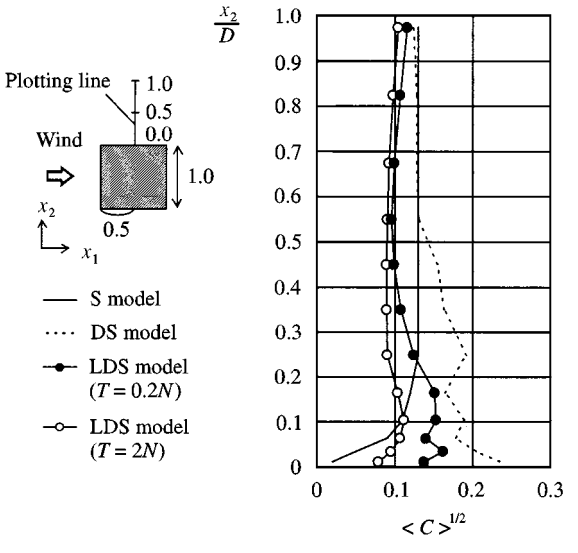

Figure 7. Comparison of model coefficient C near the side-face.

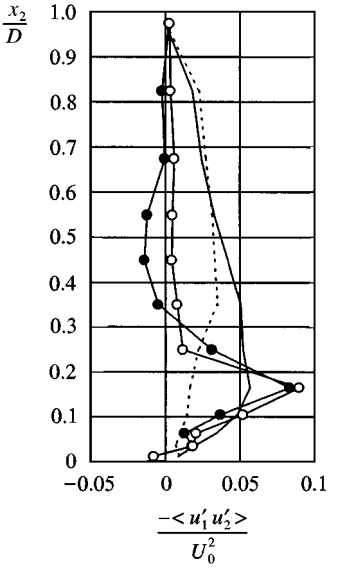

Figure 8. Comparison of shear stress $-\langle u_1' u_2' \rangle$ near the side-face.

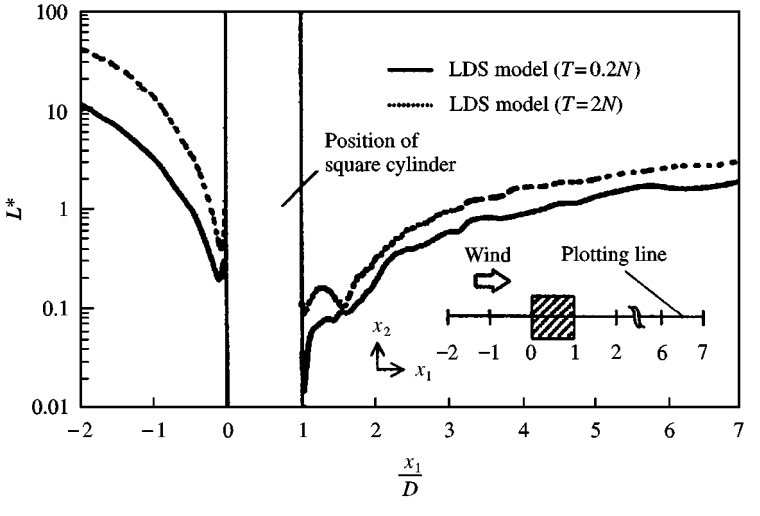

Figure 9. Distribution of the integration length L^*, along the centreline (normalized by D).

S and DS models. This difference is closely related to the difference of the position of the eddy centre between the LDS models and the other models, as described above.

4.2.5. *The length of integration along flow path-line*

Figures 9 and 10 show the length of integration along the flow path-line, L^* (normalized by D), which is controlled by T in the LDS models. The value of L^* is obtained as the length

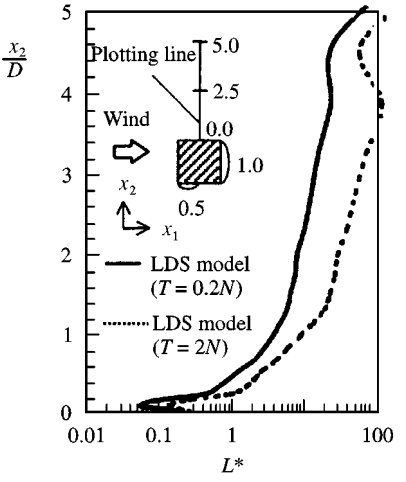

Figure 10. Distribution of L^* near the side-face.

interval over which the integrated value of weighting function becomes 90% of the total integral (from $-\infty$ to t). Figures 9 and 10 compare the distribution of L^* for the cases of $T = 2N$ and $T = 0{\cdot}2N$ in the x_1 and x_2 directions, respectively. It is seen in these figures that L^* in the case with $T = 2N$ is twice or three times larger than that in the case with $T = 0{\cdot}2N$ in the region near the cylinder. As shown in Figure 10, L^* in the case of $T = 2N$ is larger than the cylinder width, $1D$, near the side face (at $x_2 = 0{\cdot}2D$), while $L^* \approx 0{\cdot}6D$ in the case of $T = 0{\cdot}2N$ at the same point. The value of L^* can be regarded to be less than $1D$ near the side face, because L^* should not exceed the extent where the property of flow can be regarded as almost similar. Therefore, the value of L^* in the case of $T = 0{\cdot}2N$ is considered more reasonable than that of $T = 2N$ for flowfield near the cylinder.

5. REMAINING PROBLEMS AND FUTURE CHALLENGES FOR APPLYING LES TO WIND ENGINEERING

As described in the foregoing, LES is a very powerful tool for predicting the flow phenomena associated with bluff body aerodynamics. In particular, the LDS model seems to be very suitable for the research concerning such flowfields since it provides good calculation stability and also good prediction accuracy. However, there still remain some problems to be solved in the future for the practical application of LES to bluff body aerodynamics.

5.1. In-Flow Boundary Condition

For the application of LES to a flowfield with obstacles, the technique for providing the in-flow boundary condition is very important since the periodic boundary condition, which has been widely used in LES applications such as channel flow cannot be used in such cases. Furthermore, the in-flow is always turbulent in wind engineering. When the in-flow is turbulent, some method for generating velocity fluctuations is required. In order to generate such velocity fluctuations, several techniques have been invented (Mochida *et al.* 1993; Lee *et al.* 1992; Kondo *et al.* 1997; Maruyama *et al.* 1997; Iizuka *et al.* 1999). The simplest method is to store the time history of velocity fluctuations given from a preliminary LES computation (Mochida *et al.* 1993). Second is the artificial generation method, in which velocity fluctuations are given by the inverse Fourier transform of a prescribed energy

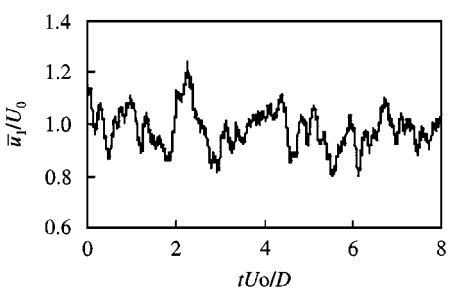

(i) Time-history of velocity $\bar{u}_1$
(streamwise component)

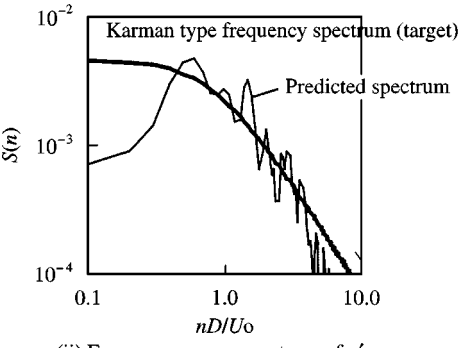

(ii) Frequency power spectrum of u_1'
given from generated inflow turbulence

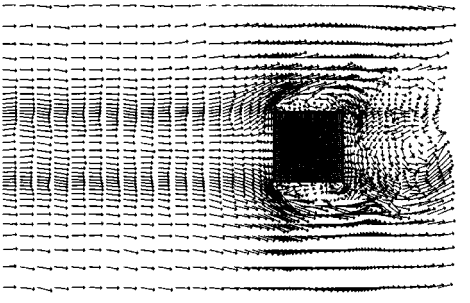

(iii) Instantaneous velocity vectors with inflow turbulence

Figure 11. Generation of velocity fluctuations with prescribed energy spectrum and turbulence intensity. (i) Time-history of velocity $\bar{u}_1$ (streamwise component) (ii) Frequency power spectrum of u_1' given from generated inflow turbulence (iii) Instantaneous velocity vectors with inflow turbulence

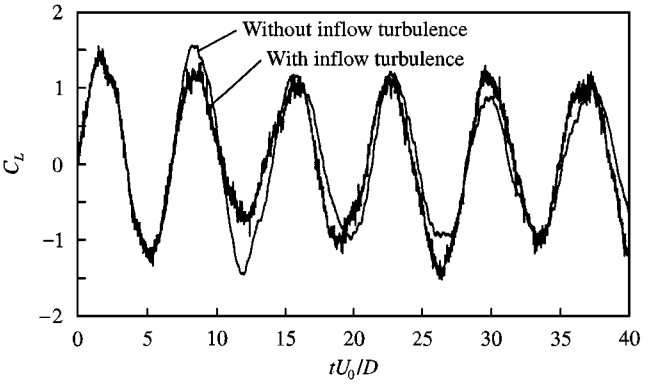

Figure 12. Comparison of time-history of lift coefficient C_L with and without in-flow turbulence.

spectrum with target turbulence intensity and length scale (Lee *et al.* 1992; Kondo *et al.* 1997; Maruyama *et al.* 1997; Iizuka *et al.* 1999). An example of velocity fluctuations given by the latter method is shown in Figure 11 (Iizuka *et al.* 1999). Here, the computation of LES is tested, based on the S model with in-flow turbulence of which turbulence level is 6%.

TABLE 2

Integral parameters

	In-flow turbulence; turbulence intensity	Reynolds number	C'_L	$\langle C_D \rangle$	St
Computation without in-flow turbulence	Smooth	$2{\cdot}2 \times 10^4$	0·86	1·99	0·135
Computation with in-flow turbulence	6%	$2{\cdot}2 \times 10^4$	0·79	1·93	0·140
Lyn (1994, 1995)	2%	$2{\cdot}2 \times 10^4$	—	2·1	0·132
Durao (1988)	6%	$1{\cdot}4 \times 10^4$	—	—	0·138
Vickery (1966)	Smooth	$1{\cdot}0 \times 10^5$	1·32	2·05	0·118
	10%		0·68	—	0·120
Lee (1975)	Smooth	$1{\cdot}8 \times 10^5$	—	2·05	—
	6·5%		—	1·93	—

Figure 12 shows a comparison of the time history of the lift coefficient, C_L, predicted in cases with and without inflow turbulence. Both results show almost the same magnitude of the amplitude of C_L. However, small perturbations are overlapped on the periodic vortex shedding fluctuations in the presence of in-flow turbulence.

Integral parameters predicted in the cases with and without in-flow turbulence are compared in Table 2 with experimental values. The r.m.s. value of lift coefficient, C'_L, and mean drag coefficient, $\langle C_D \rangle$, predicted by the case with in-flow turbulence are lower than those of case without inflow turbulence. The effect of inflow turbulence is found to decrease these values. The value of Strouhal number, St, on the contrary, becomes larger as the inflow turbulence level is increased. These tendencies also appear in the experimental results (Lyn & Rodi 1994; Lyn *et al.* 1995; Durao *et al.* 1988; Vickery 1966; Lee 1975). The results in the computations generally agree with the experimental trends.

Since the treatment of the turbulent in-flow boundary condition is a very important subject for wind engineering applications, more attention and effort should be devoted to this technique.

5.2. NEAR-WALL TREATMENT

In wind engineering problems, Reynolds numbers are usually very large. This makes it very difficult to use the non-slip boundary condition at a solid wall. Thus, the adoption of a macroscopic boundary condition, i.e., some wall function, is necessary in CFD applications to bluff body aerodynamics. In recent years, the present authors have used the Werner and Wengle type wall boundary condition which assumes a linear or power law distribution of the instantaneous velocity just near the wall according to the value of x_n^+ (Werner and Wengle 1991):

$$\frac{\bar{u}}{u_*} = x_n^+ \quad \text{when } x_n^+ \leq 11{\cdot}81\text{: linear law (non-slip)}, \tag{6}$$

$$\frac{\bar{u}}{u_*} = 8{\cdot}3 x_n^{+\,1/7} \quad \text{when } x_n^+ > 11{\cdot}81\text{: power law}. \tag{7}$$

It should be noted that this wall boundary condition becomes completely identical to the non-slip boundary condition when $x_n^+ \leq 11{\cdot}81$. Therefore, this boundary condition should be called an "extended" non-slip boundary condition.

6. CONCLUSIONS

This paper reviews recent developments in LES application to bluff body aerodynamics. One of the most important achievements in LES research in recent years seems to be the development of the dynamic type LES. The dynamic SGS model (DS model) improves the prediction accuracy remarkably in comparison with the result of the standard Smagorinsky model (S model), but computations tend to be unstable when it is applied to the flow past bluff bodies.

To correct this drawback of the DS model, a method for stabilization by averaging over particle trajectories employed by the Lagrangian dynamic SGS model (LDS model) is very useful. This technique can contribute to a remarkable improvement of calculation stability and also to the improvement of prediction accuracy when an appropriate value is selected for the time scale for Lagrangian averaging.

We conducted two cases of LDS model computations in order to investigate the effect of the time scale T, which corresponds to the integral interval along the flow path line. One is the case of $T = 2N$ optimized by Meneveau *et al.* (1994) for isotropic turbulence, and the other is the test case of $T = 0{\cdot}2N$. Within the experience of our group, the LDS model with $T = 0{\cdot}2N$ provides more reasonable results than does the case with $T = 2N$. This means that the appropriate value of T for flow past bluff body is different from that for isotropic turbulence studied by Meneveau *et al.* (1994).

There still remain some problems to be resolved for practical applications of LES. One of the most important of such problems is related to the treatment of velocity fluctuations at the in-flow boundary. An example of the results based on the artificial method for generating in-flow turbulence is presented in this paper.

ACKNOWLEDGEMENT

The authors would like to express their gratitude to Professor A. Mochida (Tohoku University, Japan) and Mr N. Tsuchiya (Research and Development Institute, Takenaka Corporation, Japan) for their valuable contribution to this work.

APPENDIX A: OUTLINE OF LAGRANGIAN MODEL

The foundation of the dynamic SGS model is the Germano identity, which is expressed as follows:

$$\mathscr{L}_{ij} = T_{ij} - \hat{\tau}_{ij} = \widehat{\bar{u}_i \bar{u}_j} - \hat{\bar{u}}_i \hat{\bar{u}}_j, \tag{A1}$$

where

$$T_{ij} = \widehat{u_i u_j} - \hat{\bar{u}}_i \hat{\bar{u}}_j, \tag{A2}$$

and where the overhat ($\widehat{\ }$) denotes the test filtering operation.

The error associated with the use of Smagorinsky model in the Germano identity is defined as

$$e_{ij}(\mathbf{x}, t) = -2C(\mathbf{x}, t) M_{ij}(\mathbf{x}, t) - \mathscr{L}_{ij}(\mathbf{x}, t), \tag{A3}$$

where

$$M_{ij} = \hat{\bar{\Delta}}^2 |\hat{\bar{S}}| \hat{\bar{S}}_{ij} - \widehat{\bar{\Delta}^2 |\bar{S}| \bar{S}_{ij}}. \tag{A4}$$

In the DS model, this local error, e_{ij}, is minimized at each time and position. In this paper, the least-squares method proposed by Lilly (1992) is used in order to minimize the square of e_{ij}.

On the other hand, the LDS model is derived by minimizing the error along fluid particle trajectories. Its trajectory for earlier times $t' < t$ is given by

$$\mathbf{z}(t') = \mathbf{x} - \int_{t'}^{t} \mathbf{u}(\mathbf{z}(t''), t'')\,\mathrm{d}t'', \tag{A5}$$

where $\mathbf{u}(\mathbf{z}(t''), t'')$ is the velocity vector at time t'' and position $\mathbf{z}(t'')$.

In the LDS model, the total error E is defined as the square of the error e_{ij} integrated from $-\infty$ to t,

$$E = \int_{-\infty}^{t} \{e_{ij}(\mathbf{z}(t'), t')\}^2\, W(t - t')\,\mathrm{d}t'. \tag{A6}$$

The weighting function, $W(t - t')$, is introduced here in order to control the relative importance of events near time t with those of earlier times. That is, the error e_{ij} at time t is weighted most strongly and the degree of weighting becomes weaker for earlier times. Thus, the definition of this weighting function determines the degree of incorporating the effect of earlier upstream information into the total error. The total error is then minimized with respect to C by the following equation:

$$\frac{\partial E}{\partial C} = \int_{-\infty}^{t} 2e_{ij}(\mathbf{z}(t'), t')\frac{\partial e_{ij}(\mathbf{z}(t'), t')}{\partial C}\, W(t - t')\,\mathrm{d}t' = 0. \tag{A7}$$

By substituting equation (A3) into equation (A7), we obtain

$$C(\mathbf{x}, t) = -\frac{1}{2}\frac{I_{LM}(\mathbf{x}, t)}{I_{MM}(\mathbf{x}, t)}, \tag{A8}$$

where

$$I_{LM}(\mathbf{x}, t) = \int_{-\infty}^{t} \mathscr{L}_{ij}(\mathbf{z}(t'), t')\, M_{ij}(\mathbf{z}(t'), t')\, W(t - t')\,dt', \tag{A9}$$

$$I_{MM}(\mathbf{x}, t) = \int_{-\infty}^{t} M_{ij}(\mathbf{z}(t'), t')\, M_{ij}(\mathbf{z}(t'), t')\, W(t - t')\,dt'. \tag{A10}$$

As to the form of the weighting function $W(t - t')$, Meneveau *et al.* (1994, 1996) proposed the use of an exponential function, $W(t - t') = T^{-1} e^{-(t-t')/T}$, because of its simplicity. In this case, I_{LM} and I_{MM} are solutions to the following relaxation-transport equations:

$$\frac{\partial \mathrm{I}_{LM}}{\partial t} + \bar{u}_i \frac{\partial I_{LM}}{\partial x_i} = \frac{1}{T}(\mathscr{L}_{ij} M_{ij} - I_{LM}), \tag{A11}$$

$$\frac{\partial \mathrm{I}_{MM}}{\partial t} + \bar{u}_i \frac{\partial I_{MM}}{\partial x_i} = \frac{1}{T}(M_{ij} M_{ij} - I_{MM}). \tag{A12}$$

Here, the time scale T controls the memory length of Lagrangian averaging and the value of T corresponds to integral period. According to Meneveau *et al.* (1994), equations (A11) and

(A12) are simplified as follows:

$$I_{LM}^{n+1}(\mathbf{x}) = \varepsilon[\mathscr{L}_{ij}M_{ij}]^{n+1}(\mathbf{x}) + (1-\varepsilon)I_{LM}(\mathbf{x} - \bar{u}^n(\mathbf{x})\Delta t), \tag{A13}$$

$$I_{MM}^{n+1}(\mathbf{x}) = \varepsilon[M_{ij}M_{ij}]^{n+1}(\mathbf{x}) + (1-\varepsilon)I_{MM}(x - \bar{u}^n(\mathbf{x})\Delta t), \tag{A14}$$

where

$$\varepsilon = (\Delta t/T^n)/(1 + \Delta t/T^n), \tag{A15}$$

and $I_{LM}^n(\mathbf{x})$, $I_{MM}^n(\mathbf{x})$ are I_{LM}, I_{MM} at position $\mathbf{x}$ and time n, respectively; $\bar{u}^n(\mathbf{x})$ is the velocity vector at position $\mathbf{x}$ and time n, and T^n is the time scale at time n.

In this paper, the form of $T = \alpha\bar{\Delta}I_{LM}^{-1/4}$ ($T = \alpha N$, $N = \bar{\Delta}I_{LM}^{-1/4}$) is adopted according to Meneveau *et al.* (1994). Here, α is a model coefficient which controls the length of T. Meneveau *et al.* (1994) recommend $\alpha = 2$, i.e. $T = 2\bar{\Delta}I_{LM}^{-1/4}$ ($T = 2N$, $N = \bar{\Delta}I_{LM}^{-1/4}$) by the optimization of α from the computational results of isotropic turbulence. The authors optimized the value of α when applying the LDS model to the flowfield around a bluff body.

APPENDIX B: NOMENCLATURE

C_D	drag coefficient
C_L	lift coefficient
C_S	Smagorinsky constant
D	width of square cylinder
$< f >$	time-averaged value of f
$\bar{f}$	grid filtered value of f
$\hat{f}$	test filtered value of f
f'	deviation from $\langle f \rangle$, $f' = f - \langle f \rangle$; in LES, $f' = \bar{f} - \langle \bar{f} \rangle$
f_μ	damping function
n	frequency
p	pressure
x_i	three components of spatial coordinate; $i = 1, 2, 3$: streamwise, lateral, vertical (or spanwise)
x_n	distance from the wall
x_n^+	$= u_* x_n/\nu$, where u_* is the friction velocity
u_i	three components of velocity vector
$\langle u_i' u_j' \rangle$	Reynolds stress
ν_{SGS}	subgrid eddy viscosity
U_0	time-averaged value of u_1 at the in-flow boundary
$S(n)$	spectrum in the frequency domain
St	Strouhal number

When values are made dimensionless, representative length scale D and velocity scale U_0 are used.

References

Akselvoll, K. & Moin, P. 1993 Large eddy simulation of a backward facing step flow. *Engineering Turbulence Modelling and Experiments* **2,** 303–313.

Antonopoulos-Domis, M. 1981 Large eddy simulation of a passive scalar in isotropic turbulent. *Journal of Fluid Mechanics* **104,** 55–79.

Biringen, S. & Reynolds, W. C. 1981 Large eddy simulation of the shear-free turbulent boundary layer. *Journal of Fluid Mechanics* **103,** 53–63.

Clark, R. A., Ferziger, J. H. & Reynolds, W. C. 1979 Evaluation of subgrid-scale models using an accurately simulated turbulent flow. *Journal of Fluid Mechanics* **91,** 1–16.

Craft, T. J. & Launder, B. E. 1992 A new model of 'Wall-Reflection' effects on the pressure-strain correlation and its application to the turbulent impinging jet. *AIAA Journal* **30,** 2970.

Deardorff, J. W. 1970 A three-dimensional numerical study of turbulent channel flow at large Reynolds numbers. *Journal of Fluid Mechanics* **41,** 453–480.

Deardorff, J. W. 1972 Numerical investigation of neutral and unstable planetary boundary layers. *Journal of the Atmospheric Sciences* **29,** 91.

Durao, D. F. G., Heitor, M. V. & Pereira, J. C. F. 1988 Measurements of turbulent and periodic flows around a square cross-section cylinder. *Experiments in Fluids* **6,** 298–304.

Germano, M., Piomelli, U., MOIN, P. & Cabot, W. H. 1991 A dynamic subgrid scale eddy viscosity model. *Physics of Fluids* **A3,** 1760–1765.

Horiuti, K. 1987 Comparison of conservative and rotational forms in Large eddy simulation of turbulent channel flow. *Journal of Computational Physics* **71,** 343–370.

Iizuka, S., Murakami, S., Tsuchiya, N. & Mochida, A. 1999 LES of flow past 2D cylinder with imposed inflow turbulence. *Proceedings of* 10*th International Conference on Wind Engineering*, Copenhagen, Denmark, 21–24 June 1999, pp. 1291–1298

Kondo, K., Murakami, S. & Mochida, A. 1997 Generation of velocity fluctuations for inflow boundary condition of LES. *Journal of Wind Engineering and Industrial Aerodynamics* **67** & **68,** 51–64.

Launder, B. E., Reece, G. J. & Rodi, W. 1975 Progress in the development of Reynolds-stress turbulence closure. *Journal of Fluid Mechanics* **68,** 537–566.

Launder, B. E. & Spalding, D. B. 1974 The numerical computation of turbulent flows. *Computational Mathematics Applied Mechanical Engineering* **3,** 269–289.

Lee, B. E. 1975 The effect of turbulence on the surface pressure field of a square prism. *Journal of Fluid Mechanics* **69,** 263–282.

Lee, S., Lele, S. K. & Moin, P. 1992 Simulation of spatially evolving turbulence and the applicability of Taylor's hypothesis in compressible flow. *Physics of Fluids* **A4,** 1521–1530.

Lilly, D. K. 1992 A proposed modification of the Germano subgrid-scale closure method. *Physics of Fluids* **A4,** 633–635.

Lyn, D. A. & Rodi, W. 1994 The flapping shear layer formed by flow separation from the forward corner of a square cylinder. *Journal of Fluid Mechanics* **267,** 353–376.

Lyn, D. A., Einav, S., Rodi, W. & Park, J. H. 1995 A laser-Doppler velocimetry study of ensemble averaged characteristics of the turbulent near wake of a square cylinder. *Journal of Fluid Mechanics* **304,** 285–319.

Maruyama, T., Rodi, W., Maruyama, Y. & Hiraoka, H. 1997 LES simulation of the turbulent boundary layer behind roughness elements using an artificially generated inflow. *The* 4*th Asia-Pacific Symposium on Wind Engineering*, volume of abstracts, 371–374.

Mason, P. J. 1989 Large eddy simulation of the convective atmospheric boundary layer. *Journal of the Atmospheric Sciences* **46,** 1492–1516.

Mason, P. J. and Derbyshire, S. H. 1990 Large-eddy simulation of the stable-stratified atmospheric boundary layer. *Boundary-Layer Meteorology* **53,** 117–162.

Meneveau, C., Lund, T. S. & Cabot, W. H. 1994 A Lagrangian dynamic subgrid-scale model for turbulence. Center for Turbulence Research, Summer Program 1994, Stanford University, 1–29.

Meneveau, C., Lund, T. S. & Cabot, W. H. 1996 A Lagrangian dynamic subgrid-scale model of turbulence. *Journal of Fluid Mechanics* **319,** 353–385.

Mizutani, K., Murakami, S., Kato, S. & Mochida, A. 1991 Study on influence of change of Smagorinsky constant. *Proceedings of Architectural Institute of Japan Annual Meeting*, pp. 483–484. (in Japanese).

Mochida, A., Murakami, S., Shoji, M. & Ishida, Y. 1993 Numerical simulation of flowfield around Texas Tech building by large eddy simulation. *Journal of Wind Engineering and Industrial Aerodynamics* **46** & **47,** 455–460.

Moin, P. & Kim, J. 1982 Numerical investigation of turbulent channel flow. *Journal of Fluid Mechanics* **18,** 341–377.

Monsour, N. N., Moin, P., Reynolds, W. C. & Ferziger, J. H. 1979 Improved methods for large eddy simulations of turbulence. In *Turbulent Shear Flows I*, p. 386.

Murakami, S., Mochida, A., Hayashi, Y. & Sakamoto, S. 1992 Numerical study on velocity-pressure field and wind forces for bluff bodies by k-ε, ASM and LES. *Journal of Wind Engineering and Industrial Aerodynamics* **41–44,** 2841–2852.

MURAKAMI, S. 1993 Comparison of various turbulence models applied to a bluff body. *Journal of Wind Engineering and Industrial Aerodynamics* **46** & **47,** 21–36.

MURAKAMI, S., MOCHIDA, A. & OOKA, R. 1993 Numerical simulation of flowfield over surface-mounted cube with various second-moment closure models. Preprint of 9*th Symposium on Turbulent Shear Flows* 13–5–1–6.

MURAKAMI, S., IIZUKA, S., MOCHIDA, A. & TOMINAGA, Y. 1997 LES analysis of turbulent flow past a square cylinder using various SGS models. *ERCOFTAC Series, Direct and Large Eddy Simulation II* (eds J.-P. Chollet, P.R. Voke & L. Kleiser), pp. 385–395.

RODI, W., FERZIGER, J. H., BREUER, M. & POURQUIE, M. 1996 Status of large eddy simulation: Results of a Workshop. *ASME Journal of Fluids Engineering* **119,** 248–262.

SCHUMANN, U. 1975 Subgrid scale model for finite difference simulation of turbulent flows in plane channels and annuli. *Journal of Computational Physics* **18,** 376–404.

VAN DRIEST, E. R. 1956 On turbulent flow near a wall. *Journal of Aeronautical Science* **23,** 1007–1011.

VICKERY, B. J. 1966 Fluctuating lift and drag on a long cylinder of square cross-section in a smooth and in a turbulent stream. *Journal of Fluid Mechanics* **25,** 481–494.

VOKE, P. R. 1997 Flow past a square cylinder: test case LES2. *ERCOFTAC Series, Direct and Large Eddy Simulation II* (eds J.-P. Chollet, P. R. Voke & L. Kleiser), pp. 355–373.

WERNER, H. & WENGLE, H. 1991 Large-eddy simulation of turbulent flow over and around a cube in a plate channel. *Proceedings of 8th Symposium on Turbulent Shear Flows*, pp. 155–168.